TR - O - 0039

28

In-Room Transmission BER Performance of Anti-Multipath Modulation PSK-VP

Hitoshi TAKAI

1991. 4. 30.

ATR光電波通信研究所

In-Room Transmission BER Performance of Anti-Multipath Modulation PSK-VP

Hitoshi TAKAI

April 30, 1991

ATR Optical and Radio Communications Research Laboratories

Abstract

This paper evaluates the BER performance of anti-multipath modulation $\pi/4$-QPSK-VP (symmetrically-mapped 4-ary PSK-VP) when applied to high-speed digital transmission within a room where both transmitting and receiving antennas are set up, and compares it with the conventional differential $\pi/4$-QPSK (symmetrically-mapped 4-ary PSK), via a transmission experiment and a calculation based on a channel model. Through this transmission experiment at about 3 and 6 Mbps, $\pi/4$-QPSK-VP is observed to improve the BER significantly over applied channels for both data-rates. Delay-profile measurement is also done using the PN correlation method and its high-resolution technique SPM. The physical channel model with only one measured parameter is proposed to explain the delay-profile measurement results. The BER calculation results based on the physical channel model are compared with the transmission experiment results, revealing that the BER calculation procedure adequately estimates the worst-case BER. The BER calculation also indicates the relationship between data-rate and BER. It is shown that $\pi/4$-QPSK-VP raises the maximum available data-rate, about 10 Mbps in an ordinary office room, about ten times over that of conventional $\pi/4$-QPSK.

H. Takai was with ATR Optical and Radio Communications Research Laboratories, Seika-cho, Soraku-gun, Kyoto 619-02, Japan. He is now with Kansai Information and Communications Research Laboratory, Matsushita Electric Industrial Co., Ltd., Moriguchi, Osaka 570, Japan.

Contents

List of Figures

List of Tables

I INTRODUCTION

Indoor high-speed digital radio communication has attracted public attention in recent years because it is a key technology in constructing a LARN (Local Area Radio Network). However, when the data-rate rises and exceeds several Mbps, severe BER (Bit Error Rate) degradation is caused by ISI (intersymbol interference) due to multipath propagation made up of radiowave reflection by walls, office fixtures, etc. In other words, multipath propagation limits the maximum available data-rate. Consequently, it greatly narrows the sphere of application.

To combat BER degradation, or raise the maximum available data-rate, various anti-multipath modulation schemes have been proposed[1]–[7], in which a redundant phase/amplitude transition/variation is imposed on a conventional modulation. In general, these schemes are characterized by *hardware simplicity* without any adaptive processes and an *excellent BER* for multipath fading whose delay differences are less than a certain value (hereafter, called the *delay difference upper limit*).

For anti-multipath modulations, the maximum available data-rate is determined by the relationship between the delay difference upper limit and the spread of the propagation channel delay-profile. In any event, a higher delay difference upper limit offers a higher available data-rate. PSK-RZ[3], with amplitude redundancy, and PSK-VP[6][7], with phase redundancy, have succeeded in raising the upper limit to almost 1 symbol and their 4-ary versions (QPSK-RZ and QPSK-VP) can nearly double the upper limit, measured in bits. These extended limits, about 1.6 to 1.7 bits, are almost the same for both modulation schemes.

If the delay difference upper limit is determined by choosing the anti-multipath modulation, then the available maximum data-rate should depend on the delay-profile of the channel. However, the actual available maximum data-rate for a practical propagation channel has not been adequately discussed. Although BER has been calculated for DSK for a Gaussian delay-profile[2], the relationship between the BER and the delay-profile based on the practical propagation channel has not been investigated. Furthermore, few transmission experiments (field tests)[8][9] have been carried out, and these were dedicated to outdoor propagation channels. None have been performed for indoor propagation channels.

In this paper, a transmission experiment was conducted to evaluate BER performance of $\pi/4$-QPSK-VP (symmetrically mapped QPSK-VP) within a room where both transmitting and receiving antennas are set up inside, in comparison with the conventional differ-

ential $\pi/4$-QPSK (symmetrically mapped QPSK). The 'in-room' BERs of $\pi/4$-QPSK-VP and $\pi/4$-QPSK were also calculated based on a simple physical channel model derived from the delay-profile measurement results, using a numerical calculation technique[7]. In-room transmission is considered essential for constructing a LARN with pico-cell architecture. Moreover, it makes the channel easy to analyze.

Although statistical channel model[10]–[12] derived from a number of delay-profile measurements may offer more accurate BER estimation, the BER calculation process tends to be complicated, requiring numerous channel measurement data. The physical channel model based on a characteristic propagation mechanism, is considered to be more significant because it can readily provide BER estimation using only a few characteristic channel parameters.

In this paper, a simple physical in-room channel model with only one measured parameter is also proposed to sufficiently explain the SPM (Superresolution PN correlation Method)[13] high-resolution delay-profile results and average power delay-profile results carried out in the same test environment[14]. The BER estimation based on the physical channel model, which is essentially a worst-case estimation, proves appropriate in comparison with the transmission experiment results. The BER estimation reveals the relationship between the BER and the data-rate.

II MODULATION AND BASIC PERFORMANCE

II.1 Modulation and Demodulation

In the transmission experiment and BER calculation, Gray-encoded symmetrically-mapped[15] 4-ary versions of differential PSK ($\pi/4$-QPSK) and PSK-VP ($\pi/4$-QPSK-VP) are compared. The symmetrically-mapped versions are more advantageous in resistance to band-limitation than the conventionally-mapped ones[15][16]. Examples of phase variation for $\pi/4$-QPSK and $\pi/4$-QPSK-VP are shown in Fig.II1.

In both modulation schemes, the phase difference θ_m between the $(m-1)$th timeslot and the m-th timeslot carries the m-th 4-ary data. Although various methods of mapping data into θ_m may be considered, θ_m were symmetrically mapped into $\pm\pi/4$ and $\pi\pm\pi/4$ by Gray encoding in this study.

In $\pi/4$-QPSK-VP, a varied phase-waveform $\phi(\epsilon)$ was redundantly imposed on the $\pi/4$-

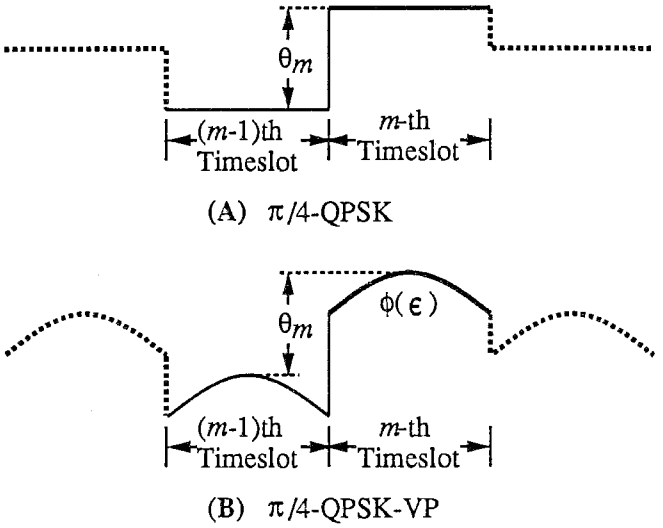

Figure II1: $\pi/4$-QPSK and $\pi/4$-QPSK-VP signal phase.

QPSK timeslot shown in Fig.II1(B). The parabolic phase-waveform, categorized into a convex phase-waveform (optimum shape to raise the delay difference upper limit[7]), was chosen and expressed as

$$\phi(\epsilon) = -4 \cdot \frac{\phi_m}{T^2} \cdot \epsilon(\epsilon - T) \,, \tag{II1}$$

where $3\pi/2$ was adopted for the maximum phase-shift ϕ_m.

To limit the bandwidth, a 50% cosine-roll-off filter was selected for $\pi/4$-QPSK and a gaussian filter (BT=2.0) was selected for $\pi/4$-QPSK-VP. Concerning demodulation, a conventional differential detector was used in both modulation schemes.

II.2 BER in 2-ray Rayleigh Fading

BER performance in 2-ray Rayleigh fading, in which two fading waves have the same average level and a delay difference τ between them, was examined through a numerical calculation and a laboratory experiment to reveal its fundamental characteristics and to verify the basic performance of the hardware used in the transmission experiment. The calculation procedure, also used in Sec.V, is the same as [7] except for band-limitation consideration. The laboratory experiment was carried out using two fading-simulators and a coaxial-cable as a delay line.

Figures II2 (i) – (ii) show BER vs. delay difference τ in terms of calculation results (curves) and laboratory experiment results (symbols) for $\pi/4$-QPSK (Fig.II2(i)) and $\pi/4$-QPSK-VP (Fig.II2(ii)). The calculation results show that the BER is significantly reduced

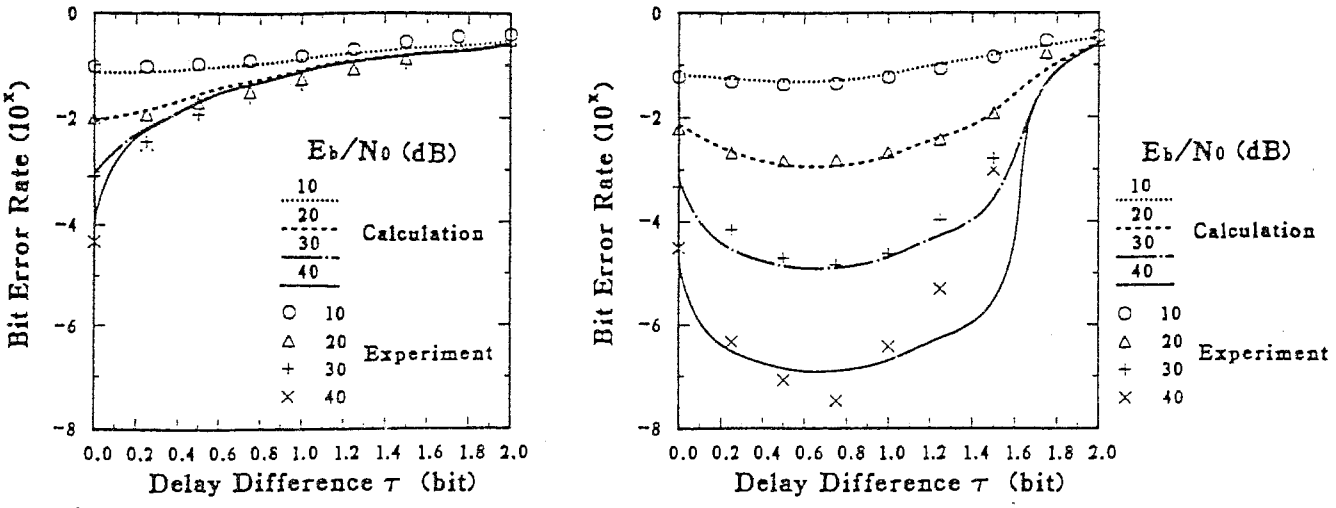

(i) for $\pi/4$-QPSK (ii) for $\pi/4$-QPSK-VP

Figure II2. BER vs. delay difference τ performance by calculation and laboratory experiment (at 6.312 Mbps) for 2-ray Rayleigh fading.

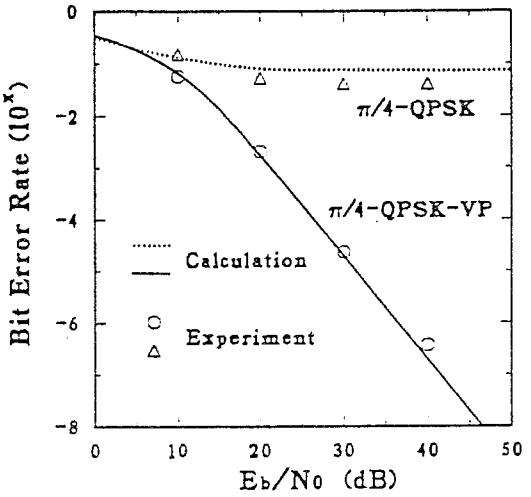

Figure II3. BER vs. SN ratio performance of $\pi/4$-QPSK and $\pi/4$-QPSK-VP by calculation and laboratory experiment (at 6.312 Mbps) for 2-ray Rayleigh fading.

for $\pi/4$-QPSK-VP in th· delay difference τ of 0 – 1.6 bits. Consequently, the delay difference upper limit, sl· ·ly degraded due to band-limitation effects in comparison with the result (about 1.7 bit ·n [7], is about 1.6 bits. The experiment results are almost in agreement with the calc· ·ion results and the measured delay difference upper limit is confirmed to be about 1.· ts. Figure II3 shows the comparison of BER vs. SN (signal to noise) ratio performance · each modulation when the delay difference τ was 1 bit. The BER of $\pi/4$-QPSK-VP is confirmed to be significantly improved.

III TRANSMISSION EXPERIMENT

III.1 Experiment Environment and Setup

The transmission experiment was conducted in an ordinary office (referred to hereafter as 'office room'), and in a shielded room. The propagation channel in the shielded room represents worst-case conditions because of the echo effect from surrounding steel shell plate walls without windows and is used for comparison. Sketch maps of both rooms with antennas set up inside are shown in Fig.III1. The basic configuration and main specifications of the BER measurement system are shown in Fig.III2 and Table III1, respectively.

In both rooms, vertically polarized dipole antennas were used for transmitting and receiving. The transmitting antenna was fixed. The receiving antenna, which was mounted on the end of a 0.93 m long pole, was rotated, and BER was averaged over one rotation. This takes about 90 s, i.e., the moving velocity V of the receiving antenna was about 6.5 cm/s.

The office room had a 2.7 m high ceiling, a free-access floor with steel underplate, a ferro-concrete outer wall without windows in the right side, a ferro-concrete outer wall with windows in the upper side, steel partition walls in the left and lower side, desks, racks, and airconditioners etc. The transmitting and receiving antennas were 2.1 m and 1.2 m high, respectively. Four measuring locations, A, B, C and D, at the centers of the rotated receiving antennas, were prepared as shown in Fig.III1.

In addition to the surrounding steel shell plates, the shielded room had inner walls made of wood and plasterboard. From the inside, it looked like an ordinary windowless room with a 2.3 m high ceiling, a free-access floor with steel underplate, desks, racks, and computers etc. The transmitting and receiving antennas were 1.2 m and 1.8 m high, respectively. Only one measuring location was prepared for this room.

Table III1: Main specifications of BER measurement system.

carrier frequency	240 MHz, 2.38 GHz
modulation	$\pi/4$-QPSK, $\pi/4$-QPSK-VP
bit rate	3.156 Mbps, 6.312 Mbps
detection	differential detection
if bandwidth	9 MHz (at -3 dB)

The experiment was carried out at bit-rates of 6.312 and 3.156 Mbps in the office room at 240 MHz band and in the shielded room at 2.3 GHz band. Fifteen-stage m-sequence pseudonoise (PN) bit sequence generated in the data generator was transmitted and received. Then, in the error detector, the received bit sequence was compared with the same internally-generated sequence bit by bit. Subsequently, bit error was detected as an output error-pulse. These pulses were totaled up by the error counter and the BER was calculated. In the transmitter, the modulation baseband signal was digitally generated by reading out a RAM (Random Access Memory) table previously written by the controller (computer). By rewriting the RAM table, the modulation type can be changed and, by varying the read-out clock rate, the data-rate can be controlled. In the receiver, a differential detector was used for both modulations. The *if* bandwidth (9 MHz) was wide enough and fixed for the data-rates and the modulations. The field strength meter was used to measure the receiving signal power simultaneously.

All measurements were done automatically by a computer set up in another room; no one was allowed to enter the test rooms. The transmitting antenna was always in line-of-sight of the receiving antenna.

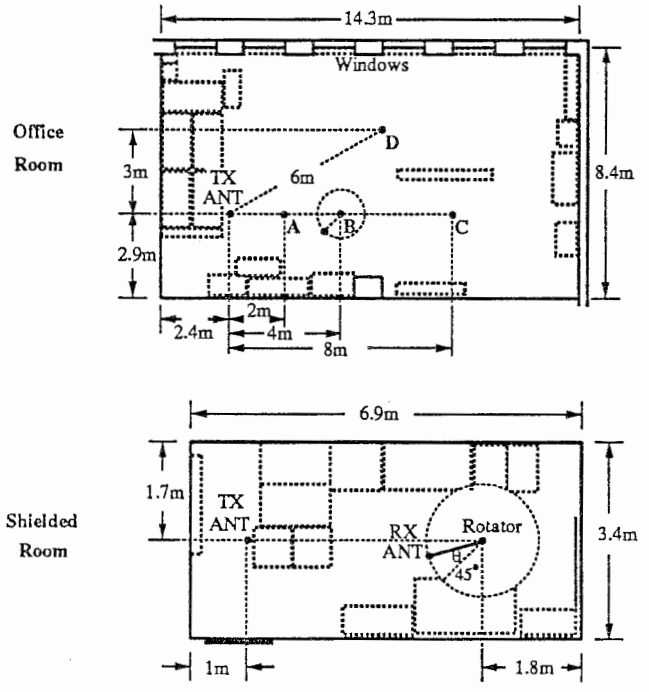

Figure III1: Sketch maps of experiment rooms and antenna set-up.

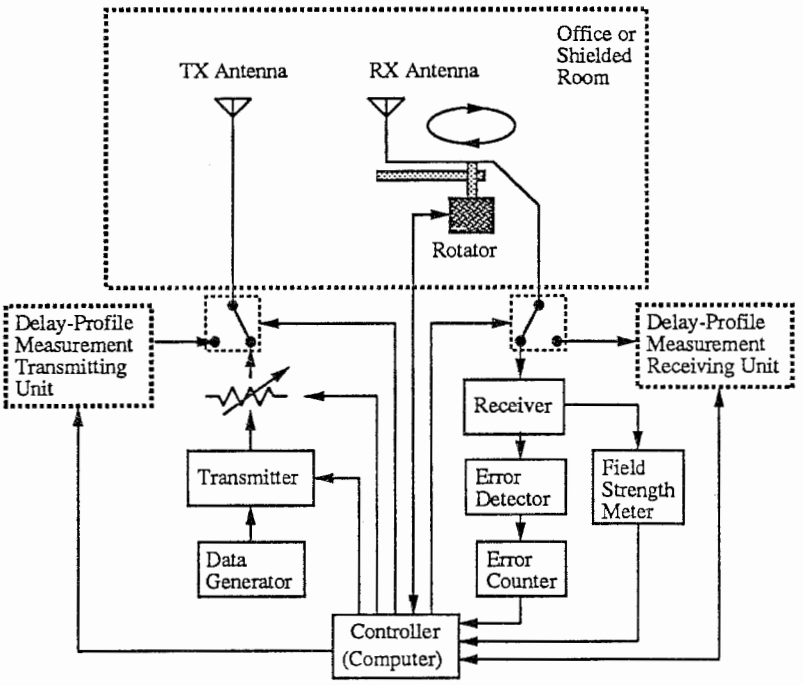

Figure III2: BER measurement system.

III.2 Transmission Experiment Result

Figures III3 (i) – (iii) show measured BER in relation to the equivalent average SN ratio at the detector input for various levels of transmitting power at measuring locations B and C in the office and shielded rooms. The equivalent average SN ratio was calculated from the receiving signal power, measured and averaged over one rotation for a given level of transmitting power and the noise figure of *rf/if* section in the receiver.

Figure III3 (i), in which the transmission range was about 4 m, shows that BER decreases suddenly when the average SN ratio increases, as in the non-fading channel, except for the case of a 6 Mbps $\pi/4$-QPSK transmission. This is because the line-of-sight (non-fading) wave was much stronger than the reflected and delayed fading waves at such close range. However, even at such close range, BER performance for conventional $\pi/4$-QPSK at the higher data-rate of 6 Mbps begins to show irreducible error due to multipath induced ISI.

On the other hand, Fig.III3(ii), in which the transmission range was about 8 m, shows that BER decreases more slowly when the average SN ratio increases, causing irreducible error, except for the case of a 3 Mbps $\pi/4$-QPSK-VP transmission. This can be explained by considering that the longer the transmission range is, the weaker the line-of-sight wave

is, relative to the reflected and delayed fading waves. Figure III3 (iii) shows that, in the shielded room, which is in a sense an echo chamber, the above BER feature has been emphasized and the irreducible error rate has become higher.

Comparing $\pi/4$-QPSK-VP and $\pi/4$-QPSK with the same data-rate, we find that the BER for $\pi/4$-QPSK-VP is significantly lower for all cases. Accordingly, the irreducible error rate is also significantly lower for $\pi/4$-QPSK-VP in comparison with $\pi/4$-QPSK. For example, at location C in the office room, where the condition was a typical middle range (about 8 m) transmission in an ordinary office, the irreducible error rates for $\pi/4$-QPSK-VP were lower 10^{-2} times (from 10^{-2} to 10^{-4}) for 6 Mbps and more than 10^{-4} times (from 10^{-3} to less than 10^{-7}) for 3 Mbps over that of conventional $\pi/4$-QPSK.

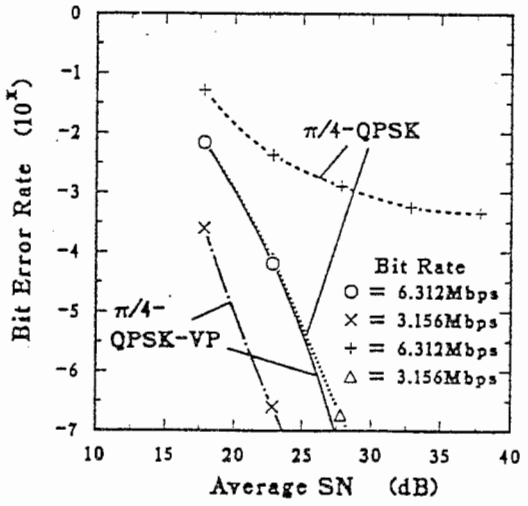

(i) at location B in office room at 240 MHz band

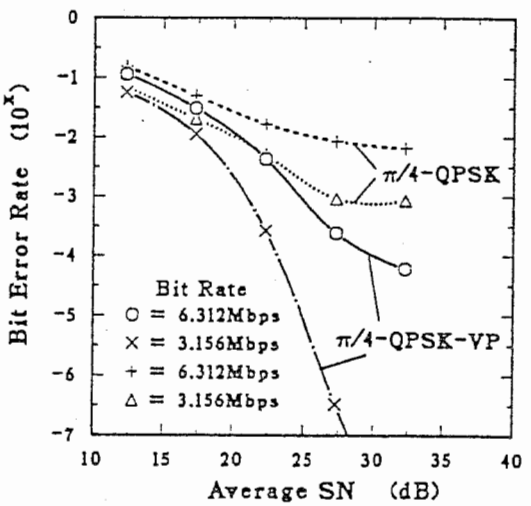

(ii) at location C in office room at 240 MHz band

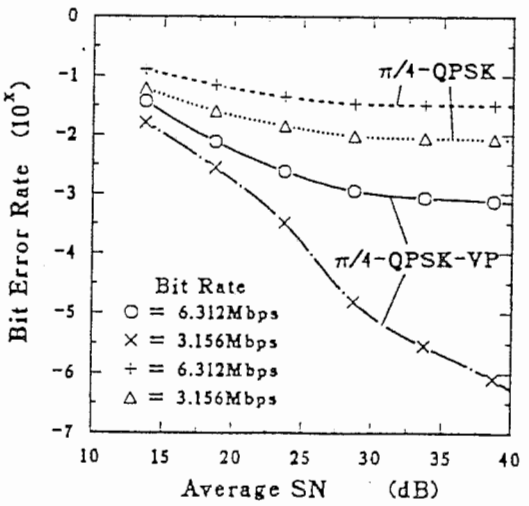

(iii) in shielded room at 2.3 GHz band

Figure III3: Transmission experiment results.

IV IN-ROOM CHANNEL MODELING

IV.1 Delay-Profile Measurement

The delay-profile measurement itself is a powerful means in analyzing the in-room propagation and deriving its channel model. The measurement was actually done using the PN correlation method[17][18] and its high-resolution technique SPM[13] for the same test environment and setup described in the previous section (cf. Fig.III1 and Fig.III2).

A block diagram of the delay-profile measurement system, used in combination with the BER measurement system as shown in Fig.III2, is shown in Fig.IV1 and its main specifications are listed in Table IV1. The system can measure delay-profiles at 910 MHz band as well as at the 240 MHz and 2.3 GHz bands described in the previous section. The basic configuration of the system is the same as that used in the conventional PN correlation method[17][18] except for the additional carrier frequency scan function, which varies the frequency of the signal generator SG1 (for 2.3 GHz band) or SG2 (for 240 and 910 MHz bands) and is necessary for SPM to decorrelate the mutual coherence of the multipath components. The PN generators in the transmitter and receiver generate identical 10-stage m-sequence. In the transmitter, the carrier is biphase-modulated by the m-sequence at a chip rate of 30 Mchips/s. In the receiver, the received signal is correlated with the identical m-sequence of a slightly lower chip rate, which enables us to obtain delay profiles via the 'sliding correlation' technique[19].

The delay-time resolution of the original delay-profile, measured as the conventional PN correlation method, is about 33 ns ($=T_c$; chip length), which corresponds to a spatial resolution of about 10 m. Considering room dimension shown in Fig.III1, there is not enough resolution for microscopic analysis; however, there is considered to be enough for macroscopic analysis. The average power delay profile, which is a macroscopic analysis,

Table IV1: Main specifications of delay-profile measurement system.

carrier center frequency	240MHz, 910MHz, 2.335GHz
carrier frequency scanning range	$\pm$20 MHz
carrier frequency scanning point	11 points (equispaced)
PN code sequence	10-stage m-sequence
chip rate T_c^{-1}	30 Mchips/s
modulation/band-limitation	BPSK / $\pm$45 MHz

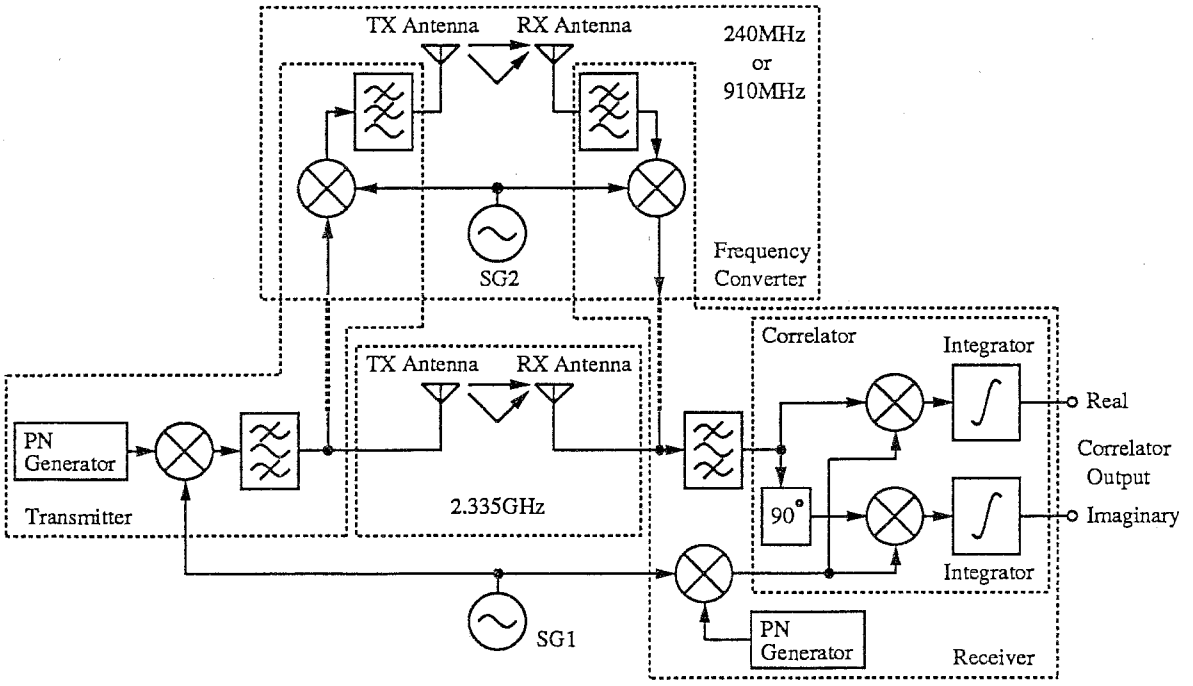

Figure IV1: Block diagram of delay-profile measurement system.

was calculated from spatially averaging the original power delay-profile over one rotation around the measurement location.

Higher delay-time resolution is needed for microscopic analysis. The SPM algorithm[13], which is based on the eigen-decomposition of the correlation matrix for the original delay-profile data vector, provides higher time resolution less than the chip length T_c. In the SPM estimation result (SPM delay-profile), several peaks indicate delay times of multi-path components with high precision, although the peak magnitudes are not necessarily in proportion to actual amplitudes of the multipath components. For two waves of the same level, the actual resolution of the above described delay-profile measurement system using SPM was about 0.2 – 0.3 T_c (7 – 10 ns), which corresponds to a spatial resolution of about 2 – 3 m as shown in [13].

IV.2 SPM Delay-Profile

The solid curves in Fig.IV2 (i) – (iii) show the typical SPM delay-profiles measured in the office room at 240 MHz, 910 MHz, and 2.3 GHz bands, respectively, when the receiving antenna was fixed at location B (the center of the circle shown in Fig.III1). The

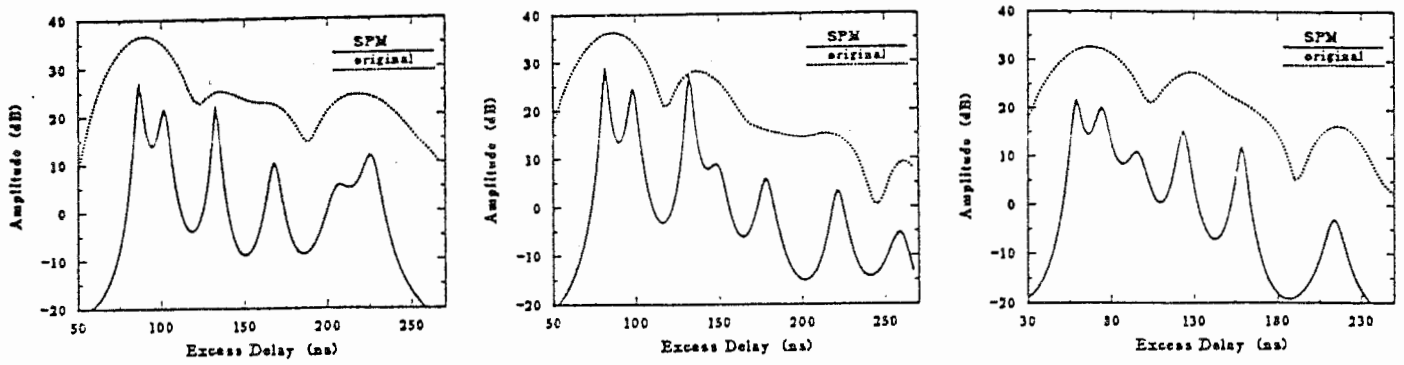

(i) at 240 MHz band (ii) at 910 MHz band (iii) at 2.3 GHz band

Figure IV2: SPM delay-profile at location B in office room.

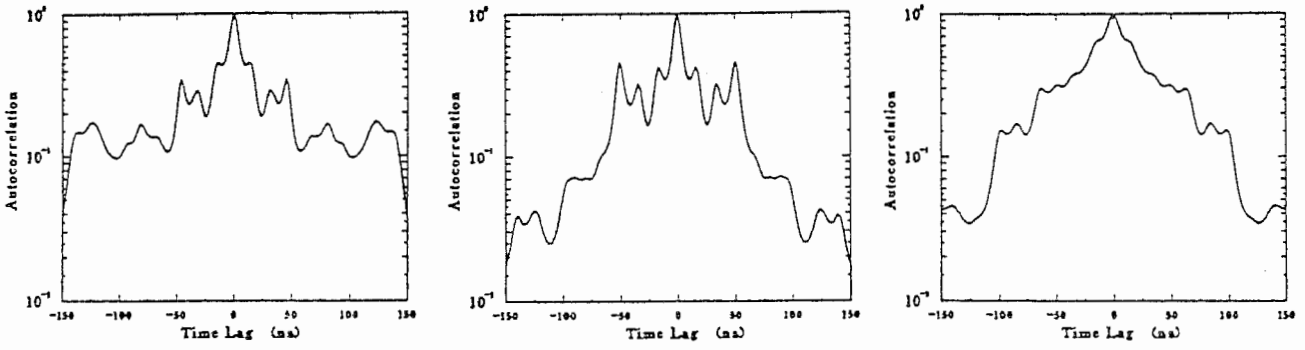

(i) at 240 MHz band (ii) at 910 MHz band (iii) at 2.3 GHz band

Figure IV3. Autocorrelation function of SPM delay-profile measured at location B in office room.

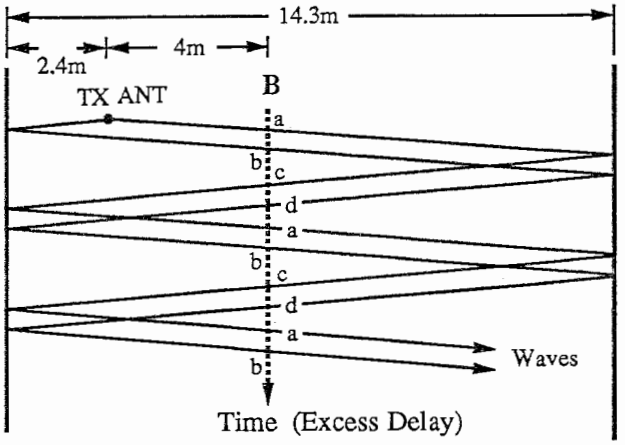

Figure IV4: Traveling diagram of reciprocating waves between opposing walls.

original delay-profiles measured by the conventional PN correlation method at the center carrier frequencies are indicated by dotted curves.

From Fig.IV2, it was found that six or seven peaks are resolved in the SPM delay-profiles (solid curves) while only three or four can be identified in the original delay-profiles (dotted curves). Furthermore, periodic structures were discovered and the peak positions relative to the first one are in agreement with these three figures, independent of the frequency band, although some peaks were missing.

The periodic structure was better understood by investigating the autocorrelation function of the SPM delay-profile shown in Figs.IV3 (i) – (iii). In all cases, it was found that a pair of nearby peaks were periodically repeated. The interval of the pair and the repetition period, which were the same in all three figures, were about 5 m and 14 m, respectively, as measured in equivalent spatial propagation length.

This periodic structure suggests the existence of multiple reflections in which waves travel back and forth between opposing walls. The wave-travel diagram in Fig.IV4 shows a pair of reciprocating waves between the left- and right-side walls from Fig.III1. At location B shown on the dotted line, reflected and delayed waves should appear at the time $a - d$ where the waves intersect the dotted line. The wave arrival time makes up the same periodic structure as found in the SPM delay-profiles. It is reasonable to assume that the reciprocating waves lose their power by a certain ratio for each reflection (including an outgoing-returning propagation loss). The delay-profile deduced from the above described *wave-reciprocation* model appears in Fig.IV5, in which the envelope of

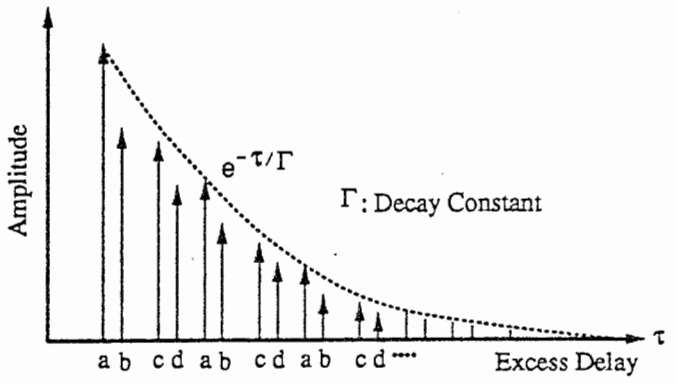

Figure IV5: Delay profile deduced from wave-reciprocation model.

multipath components exponentially decays according to the excess delay and wave arrival time forms the periodic structure. From the geometrical setup, the interval of the pair waves is 4.8 m and the repetition period is estimated at about 14.3 m by considering that location B is almost the middle point between the walls. The deduced results coincide well with the measured results.

IV.3 Average Power Delay profile

The wave-reciprocation/exponential-decay phenomenon is also supported by average power delay profile results. Figures IV6 (i) – (ii) show the spatial averages of the original power delay profiles measured at every 1 degree of rotation, around the locations at A through

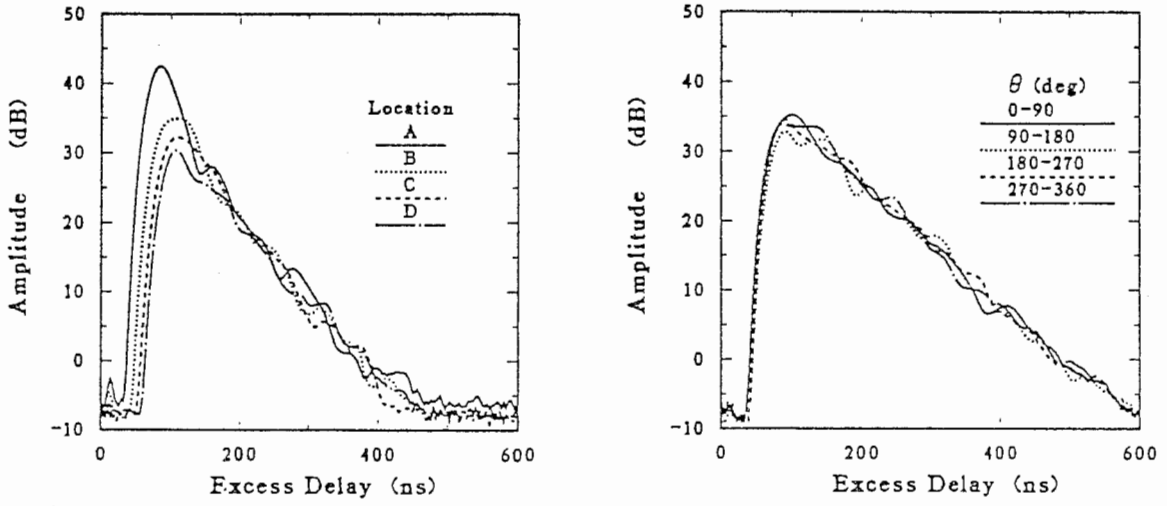

(i) in office room at 240 MHz band (ii) in shielded room at 2.3 GHz band

Figure IV6: Average power delay profile.

D in the office room at 240 MHz band and over four partitioned circles in the shielded room at 2.3 GHz band, respectively. Except for the left-side peak, which is considered the line-of-sight wave, in the case of nearby transmission in the office room (location A and B), we find that the right-side tails of all results drop almost in a straight line, i.e., the multipath component levels exponentially decrease according to the excess delay.

Furthermore, it was noted that the decay constant was the same independent of the location in each room. That is, the radiowave energy emitted by the transmitting antenna at a certain time, exponentially decayed at the same rate everywhere in the room. This indicates that the room can be modeled as a cavity. The decay constant or the Q-factor of the cavity is an important parameter in characterizing the channel. The measured decay constants from the tail slope in Fig.IV6 were 0.11 dB/ns for the office room and 0.088 dB/ns for the shielded room. As actually found in the transmission experiment, the shielded room is more echoic and worse for high-speed data transmission than the office room.

IV.4 In-room Channel Modeling

The phenomenon of the wave reciprocation between opposing walls was also observed using a directional antenna[20]. In general, many reciprocating routes (for example, between two opposing walls, ceiling and floor, corner and corner) are considered to exist. However, in this measurement, the simplest model with one dominant route, where the decay constant is considered the lowest, is sufficient to explain the periodic structure found in the SPM delay-profile.

In an SPM algorithm, waves are identified in order of their power levels. Closely-adjacent waves within the time-resolution are identified as one wave[13]. A wave which is identified by using SPM may be made up of several waves close together caused by additional floor reflection or wall roughness, etc. Weaker waves may be neglected. Only the main characteristics of the channel are emphasized, hense, a simple model is made.

This simplest model h[illegible] also been supported by exponentially decaying average power delay profiles. Furtherm[illegible] the average delay profile results reveal that the decay constant is a characteristic param[illegible]r for a room independent of location. So far as is known, no previous work has clearl[illegible]alt with this point. In general, the delay spread is thought to be closely related to [illegible] decay constant. However it is somewhat difficult to use the delay spread to estimat[illegible]he decay constant for a line-of-sight propagation because a conspicuous line-of-sight wave has a great influence on the measured delay spread.

The delay-profile deduced from the *wave-reciprocation/cavity* model is characterized by a periodic arrival structure and exponential decay according to excess delay (Fig.IV5). The characteristics do not coincide with that of Saleh's model[10] in which waves arrive in clusters and both clusters and waves in the clusters exponentially decay with different constants and form Poisson arrival process. This difference is considered to be derived from that Saleh's model mainly deals with the transmission between room and hallway in contrast to in-room transmission. The clusters in Saleh's model are considered to be the results of resonance in each room. A simpler model is possible for the in-room transmission channel because the other room resonances are considered to have little effect on the channel.

In concluding generally, the analyses for only two rooms (the office and shielded rooms) may be insufficient, however, at least, the *wave-reciprocation/cavity* model can sufficiently explain the delay-profile results measured in them.

V BER ESTIMATION BASED ON IN-ROOM CHANNEL MODEL

V.1 BER Calculation

BER was calculated based on the *wave-reciprocation/cavity* model described above. For actual calculation, some simplifications and assumption were added. Figure V1 shows the delay profile used in the calculation.

The periodic arrival time structure shown in Fig.IV5 was simplified into the peri-

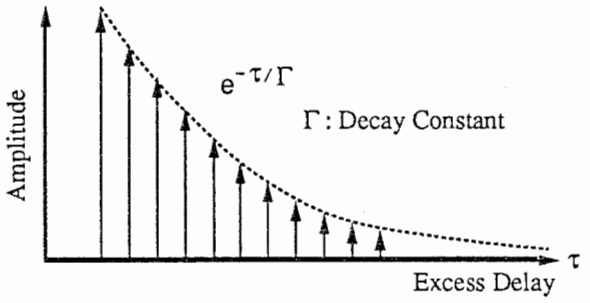

Figure V1. Channel model used in BER calculation (equispaced and exponentially decaying 11-ray Rayleigh fading model).

odic/equispaced structure in Fig.V1. The spacing between adjacent waves was 30 ns (9 m in space) and the first 11 waves were taken into account. There was no solid basis for designating the simple periodic structure, the spacing and the number of waves. However, the calculated BERs were observed to be little affected by the detailed arrival time structure if more than about 5 waves were taken into account.

In the calculation, each multipath component, for which average power level exponentially decays with decay constant Γ according to excess delay, was assumed to be subjected to independent Rayleigh fading. Obviously, a line-of-sight wave, observed as a peak in the average power delay profile for nearby transmission (Fig.IV6), is not subjected to fading. Consequently, the BER calculation based on the assumption is essentially a worst-case estimation.

The decay constant Γ was the only measured parameter. It was 0.11 dB/ns for the office room and 0.088 dB/ns for the shielded room as described in the previous section. The maximum Doppler frequency f_D is another parameter of the channel model and is calculated from the moving velocity V of the receiving antenna and the wavelength λ as

$$f_D = \frac{V}{\lambda} . \qquad \text{(V1)}$$

In comparison to the transmission experiment results, the moving velocity V was assumed to be the same as that in the experiment (6.5 cm/s). Then, from Eq.V1, the maximum Doppler frequency f_D was calculated as 0.52 Hz for the 2.3 GHz band, or 0.052 Hz for the 240MHz band.

The calculation was done by a numerical technique utilizing a characteristic function. The actual calculation process is the same as [6] except that the band-limitation effect is also considered.

V.2 Calculation Results

Figures V2 (i) – (ii) show the calculation results for the office room at the 240 MHz band and for the shielded room at the 2.3 GHz band.

Comparing the calculation results in Fig.V2(i) and the transmission experiment results in Fig.III3(ii) for the office room, where the transmission range was about 8 m, we find that both results are similar though the irreducible error rate from the experiment is slightly better than that from the calculation. However, for shorter transmission range (about 4 m), comparing Fig.V2(i) and Fig.III3(i), the BER from the experiment is far better than that from the calculation. This is because the non-fading line-of-sight wave,

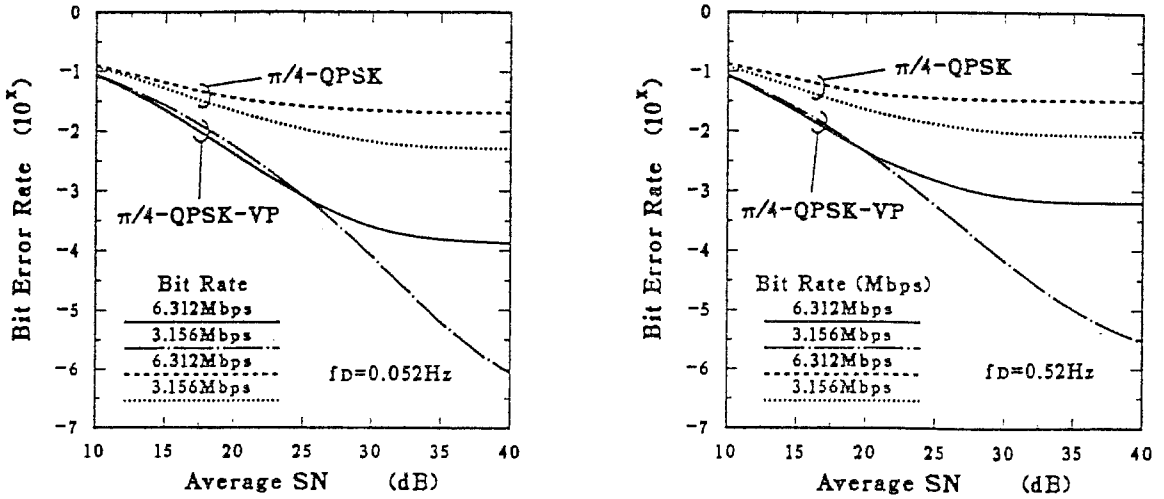

(i) in the office room at 240 MHz band (ii) in the shielded room at 2.3 GHz band

Figure V2: BER calculation result.

which is the more conspicuous for the shorter transmission range, was also assumed to be subjected Rayleigh fading in the calculation process.

Comparing the calculation results in Fig.V2(ii) and the transmission experiment results in Fig.III3(iii) for the shielded room, we find that both results, in particular, the irreducible error rates are in agreement. As shown in Fig.IV6, the shielded room was more echoic and the non-fading line-of-sight wave was not conspicuous in comparison with strong reflected waves. For such inferior case, the BER calculation process is confirmed to provide a more precise BER estimation. Conversely, the agreement is evidence for the appropriateness of the channel model on which the calculation was based.

V.3 Data-Rate and BER

The calculation also reveals the relationship between data-rate and BER. Figure V3 shows the comparison of the BERs for $\pi/4$-QPSK-VP and conventional $\pi/4$-QPSK, for sufficiently high SN ratio (50 dB) and the decay constant measured in the office room (0.11 dB/ns). If the transmitting power is sufficient, we find that $\pi/4$-QPSK-VP significantly improves the BER over the data-rate from several hundred kbps to several Mbps in comparison with conventional $\pi/4$-QPSK. An optimum bit-rate, about 2 Mbps for the office room, exists for $\pi/4$-QPSK-VP and minimizes the BER to 10^{-8}. The maximum available data-rate is estimated to be about 10 Mbps for an allowable BER of 10^{-3} for the office room.

For a different decay constant, the relationship, as shown in Fig.V3, only shifts along the bit-rate-axis, expressed in logarithm, keeping its shape of curves. For example, in the

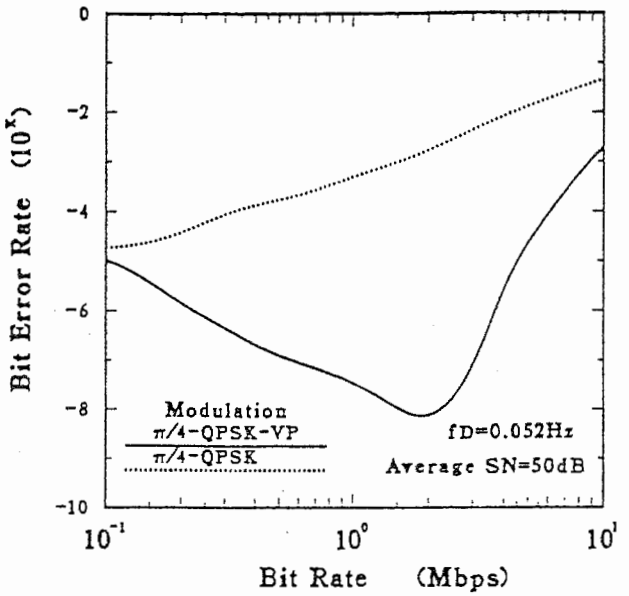

Figure V3. Relationship between data-rate and BER when the decay constant is 0.11 dB/ns (measured in office room).

shielded room, because the decay constant (0.088 dB/ns) is smaller by 20% than that in the office room, the curves in Fig.V3 shift to the left by 20% in bit-rate. Consequently, the optimum bit-rate becomes about 1.6 Mbps and the maximum available bit-rate becomes 8 Mbps.

For various decay constants, at least, we can conclude that $\pi/4$-QPSK-VP raises the maximum available data-rate about ten times over that of conventional $\pi/4$-QPSK when BER ranges from 10^{-3} to 10^{-4}.

VI CONCLUSION

For in-room propagation channels, significant BER improvement and the consequent rise of the available maximum data-rate for $\pi/4$-QPSK-VP in comparison with conventional $\pi/4$-QPSK have been observed through a transmission experiment and a calculation based on a physical channel model.

For about 8 m transmission experiment in the office room, the irreducible error rates of $\pi/4$-QPSK-VP were reduced to 10^{-4} for 6 Mbps and to less than 10^{-7} for 3 Mbps, which were 10^{-2} times and more than 10^{-4} times over that of conventional $\pi/4$-QPSK. 6 Mbps transmission was possible by using $\pi/4$-QPSK-VP with a BER of 10^{-4}.

Delay-profile measurements, carried out for the same test propagation channels, has revealed in-room propagation and enabled us to construct a simple physical channel model.

SPM delay-profile has revealed the existence of reciprocating waves between opposing walls through the periodical arrival time structure. The wave-reciprocation/exponential-decay phenomenon has also been supported by average power delay-profile results with exponentially decaying tails. These results have also indicated that the decay constant, measured as the tail slope, is characteristic of the room independent of location inside, as if the whole room were a cavity. The BER calculation was done based on an equispaced/exponentially-decaying 11-ray Rayleigh fading model, which is deduced from the *wave-reciprocation/cavity* model with only one measured parameter, i.e., decay constant.

The BER calculation is essentially a worst-case estimation due to assuming a non-fading line-of-sight wave as a Rayleigh fading wave. As actually confirmed in comparison with the transmission experiment results, the BER calculation process provides a good estimation for the worst-case BER. For longer range transmission, the experiment results have been observed to approach the calculation results. For the shielded room, where echo effect prevents a conspicuous line-of-sight wave, both results have been observed to be in agreement. The worst-case BER estimation is considered indispensable for the practical applications. Noting that it can be done using only one measured parameter, the BER estimation process is considered very useful.

From the BER calculation, the relationship between data-rate and BER has been revealed. If the transmitting power is sufficient, $\pi/4$-QPSK-VP significantly reduces the BER over the data-rate from several hundred kbps to several Mbps in comparison with conventional $\pi/4$-QPSK. An optimum bit-rate, about 2 Mbps for the office room, exists for $\pi/4$-QPSK-VP and minimizes the BER to 10^{-8}. The maximum available data-rate has been estimated to be about 10 Mbps for an allowable BER of 10^{-3} for the office room. Although the relationship expands or shrinks along the bit-rate-axis for different decay constants, it can be concluded that $\pi/4$-QPSK-VP significantly raises the maximum available data-rate about ten times over that of conventional $\pi/4$-QPSK when BER ranges from 10^{-3} to 10^{-4}.

Acknowledgments

The author wishes to extend special thanks to Takeshi Manabe (CRL) for developing the SPM delay-profile measurement technique and for his earnest discussions about indoor channel modeling. The author is greatly indebted to Tokio Taga (NTT), Hiroyuki Imahori (Kyocera) and Eiichi Ogawa (ATR) for installing the delay-profile measurement system. Thanks is also due to Keigo Iizuka (Univ. of Toronto) and Wataru Matsui (ATR) for

their helpful suggestions on indoor channel modeling. The author also wishes to express sincere appreciation to Yoji Furuhama, Masami Akaike and other staff of ATR Optical and Radio Communications Research Laboratories for their continuous encouragement during this research project.

Bibliography

[1] J. Horikoshi, "Error performance considerations of $\pi/2$-TFSK under the multipath interfering environment," *Trans. IECE Japan*, vol. E67, No. 1, pp. 40 – 46, Jan. 1984.

[2] S. Ariyavisitakul, S. Yoshida, F. Ikegami, and T. Takeuchi, "A novel anti-multipath modulation technique DSK," *IEEE Trans. Commun.*, vol. COM-35, No. 12, pp. 1252 – 1264, Dec. 1987.

[3] S. Ariyavisitakul, S. Yoshida, F. Ikegami, and T. Takeuchi, 'A proposal of an anti-multipath modulation technique PSK-RZ', *Papers, Tech. Group Commun.*, IECE Japan, CS85-155, Jan. 1986.

[4] H. Takai, "A proposal of an anti-multipath modulation technique," *Papers, Tech. Group Commun.*, IECE Japan, CS86-48, Sept. 1986.

[5] S. Yoshida and F. Ikegami, "Anti-multipath modulation technique — Manchester-coded PSK (MC-PSK) —," in *Proc. IEEE ICC'87*, pp. 39.3.1 – 39.3.5, Seattle, June 1987.

[6] H. Takai, "BER performance of anti-multipath modulation PSK-VP and its optimum phase-waveform," in *Proc. IEEE VTC'90*, pp. 412 – 419, Orlando, May 1990.

[7] H. Takai, "BER performance of anti-multipath modulation scheme PSK-VP and its optimum phase-waveform," submitted to *IEEE Trans. Veh. Technol.*

[8] T. Takeuchi, F. Ikegami, S. Yoshida and N. Kikuma, "Comparison of multipath delay characteristics with BER performance of high speed digital mobile transmission," *Proc. IEEE VTC'88*, pp. 119 – 126, , June 1988.

[9] S. Yoshida, T. Takeuchi, M. Nakamura and F. Ikegami, "High bit-rate field transmission of an anti-multipath modulation technique PSK-RZ," *Proc. IEEE VTC'90*, pp. 527 – 532, Orlando, May 1990.

[10] A. M. Saleh and R. A. Valenzuela, "A statistical model for indoor multipath propagation," *IEEE J. Selec. Areas Commun.*, vol. 5, no. 2, 1987.

[11] T. S. Rappaport, "Characterization of UHF multipath radio channels in factory buildings," *IEEE Trans. Antennas Propagat.,* vol. AP-37, no. 8, pp. 1058 – 1069, 1989.

[12] S. Y. Seidel and T. S. Rappaport, "Simulation of UHF indoor radio channels for open-plan building environments," in *Proc. IEEE VTC'90*, pp. 597 – 602, Orlando, May 1990.

[13] T. Manabe and H. Takai, "Superresolution of multipath delay profiles measured by PN correlation method," submitted to *IEEE Trans. Antennas Propagat.*

[14] H. Takai and T. Manabe, "An indoor propagation analysis using delay profiles measured by the superresolution pulse-compression method," presented at 1991 North American Radio Science Meeting and International IEEE/AP-S Symposium, London, Ontario, Canada, June 1991.

[15] J. H. Winters, "Differential detection with intersymbol interference and frequency uncertainty," *IEEE Trans. Commun.*, vol. COM-32, No. 1, pp. 25 – 33, Jan. 1984.

[16] H. Takai, "Band-limitation effect for anti-multipath modulation scheme PSK-VP," to be submitted to *Trans. IECE Japan.*

[17] D. C. Cox, "Delay Doppler characteristics of multipath propagation at 910 MHz in a suburban mobile radio environment," *IEEE Trans. Antennas Propagat.*, vol. **AP-20**, no. 5, pp. 625 – 635, Sept. 1972.

[18] D. M. J. Devasirvatham, "Time delay spread and signal level measurements of 850 MHz radio waves in building environments," *IEEE Trans. Antennas Propagat.,* vol. AP-34, no. 11, pp. 1300 – 1305, Nov. 1986.

[19] D. C. Cox, "910 MHz urban mobile radio propagation: Multipath characteristics in New York City," *IEEE Trans. Commun.*, vol. COM-21, pp. 1188 – 1194, Nov. 1973.

[20] T. Takeuchi, M. Sako and S. Yoshida, "Multipath delay estimation for indoor wireless communication," in *Proc. IEEE VTC'90*, pp. 401 – 406, Orlando, May 1990.